Spatially Resolved Measurements of the Chromatic Dispersion in Fibers

Evgeny Myslivets and Stojan Radic

(Invited Tutorial)

***Abstract*—Technique for selective localization of four-photon mixing and its use for physical parameter extraction in fiber is described. The measurement method relies on localized counter-colliding power transfer and was applied to map dispersion and corresponding transverse geometry of different types of optical fibers. The technique is capable of resolving fiber core fluctuations comparable to a single silica molecular diameter.**

***Index Terms*—Dispersion fluctuations, four wave mixing (FWM), nonlinear fiber, parametric gain.**

I. Introduction

THE introduction of the silica-based nonlinear fibers in early 1990s initiated a new area of research in nonlinear optics and provided both practical and fundamental advantages over traditional nonlinear optical effects in bulk media [1]–[4]. Subsequently, the fiber nonlinear optics has evolved into a distinct discipline that relies on manipulation of guided modes that interacted via nonlinear silica response. Fiber platform could fully rely on temporal formalism in which the strength of the nonlinear effects is defined by unique transversal modes, eliminating beam alignment considerations and complex spatio-temporal analysis in a bulk nonlinear media. In practical sense, the analysis of nonlinear effects in single- and few-mode fibers addresses much simpler propagation of the interacting waves represented by their temporal waveforms.

In comparison to centimeter-long crystalline devices ([4, Fig. 2.1]), weaker fiber (silica) nonlinearity ($\sim 3 \cdot 10^{-16}$ cm^2/W) is compensated by significantly longer interaction length. Measurements in high-confinement fibers have demonstrated that strong nonlinear interaction can occur over hundreds of meters and achieve efficiencies in excess of 50 dB [5]. Practical difference between crystal and fiber device originates with inherent nature of its nonlinear response. Specifically, doped silica glasses used for fibers do not possess significant second order nonlinearity $\chi^{(2)}$, while having only relatively weak third order nonlinearity ($\chi^{(3)}$). Furthermore, since the transversal degree of freedom associated with spatial (polarization) alignment is eliminated, the efficiency of nonlinear interaction is governed by the longitudinal phase matching ([3]) and defined by the chromatic dispersion of the interacting modes. The net chromatic dispersion experienced by a mode is a result of material polarizability and waveguide geometry. The effective fiber nonlinearity, defined by a mode nonlinear coefficient γ, is inversely proportional to a modal effective area A_{eff} ([3, Eq. (2.3.30)]) that is closely related to the size of the mode. In simple terms—any increase in effective fiber nonlinearity should be accomplished in close concern with dispersive engineering [6]. This optimization process becomes a considerable challenge when device must possess wide spectral response. In this case, high modal confinement must be combined with precise dispersive engineering that extends beyond dispersion and dispersion slope. As a result, the performance of parametric fiber devices rests completely on the ability to *design* and *measure* fiber parameters with tightly controlled modal confinement and chromatic dispersion.

Unfortunately, even with optimal fiber design, the fabrication process results only in the approximation of target fiber characteristics. Microscopic variations in transverse fiber geometry and doping concentration [7] lead to spatially localized dispersion fluctuations. While such fluctuations are not critical in case of fibers designed for transmission, they impose fundamental limitation on fibers specifically designed for nonlinear device construction. As an example, in case of a conventional single mode fiber (SMF), the acceptable core size variance leads to zero-dispersion-wavelength (ZDW) fluctuation in excess of 10 nm, or equivalently, random dispersive shift of $\sim$1 ps/nm/km along the fiber [8]. In addition, the dispersion properties are also affected by the external, post-fabrication factors such as strain and temperature [9]. Similar, relaxed tolerance on dispersion cannot be accepted for nonlinear applications. Instead, the construction of wideband nonlinear device mandates both high confinement and sub-nm ZDW variations [7]. In physical nonlinear fibers, ZDW variations easily exceed this requirement, resulting in spatially varying phase matching condition that qualitatively decreases nonlinear efficiency. Stochastic geometry fluctuation was identified as the leading obstacle on a path to realization of wideband and efficient parametric mixers.

In most demanding mixer designs, small dispersion fluctuations require transverse fabrication tolerances of only *few nanometers*, comparable to a molecular dimension of silicon-oxygen molecular manifold. While such requirements can be arguably viewed as unphysical, a relaxed fabrication standard cannot lead to useful performance. In case of the conventional highly nonlinear fibers (HNLF), only 1% (= 16 nm) variation in the core radius ($r \sim 1.6$ μm) results in 30-nm shift of ZDW [7].

Manuscript received August 25, 2014; revised October 20, 2014; accepted October 22, 2014. Date of publication December 30, 2014; date of current version February 17, 2015.

The authors are with the Department of Electrical and Computer Engineering, University of California, San Diego, CA 92093 USA (e-mail: ymyslive@ucsd.edu; sradic@ucsd.edu).

Color versions of one or more of the figures in this paper are available online at http://ieeexplore.ieee.org.

Digital Object Identifier 10.1109/JLT.2014.2369343

With recent progress in fabrication process, it is now possible to substantially reduce ZDW fluctuations. However, it does not appear that HNLF fabrication with molecular-scale precision is viable, suggesting the search for alternative means for longitudinal phase matching control. This example illustrates that the dispersion or ZDW is an extremely sensitive parameter of the transversal geometry. The opposite statement is also valid: if one could accurately characterize dispersion along the fiber coordinate, one could predict the transversal geometry with nanometer precision.

The typical applications of the nonlinear fibers include parametric amplification [10], wavelength conversion [11], multi-casting [12], [13], all-optical regeneration [14], pulse compression [15], high-speed switching [16], de-multiplexing [17], photon switching [18], sampling [19], comb [20] and supercontinuum generation [21], short-pulse generation [22], and soliton-related applications [23]. It is necessary to emphasize that most of applications utilizing continuous-wave (CW) pumping do not require power levels exceeding several Watts and lengths longer than several hundred of meters, whereas, in pulsed regime, the typical lengths are at the range of tens of meters. In practical terms, each application dictates target dispersion precision: some of them need ultra-stable longitudinal dispersion, the others need "heterogeneous" designs composed several dispersion- and nonlinear-dissimilar stages (for example, [12] and [24]). In typical application, parameters of primary concern are parametric (generation/amplification) efficiency and operational bandwidth. In many cases, fibers need an accurate dispersion characterization along the entire interaction length. If longitudinally resolved dispersion is known with sufficient accuracy, one could select specific parts of the fiber and splice these in particular order to satisfy the target requirements for the device response. In an alternative strategy, the specific concatenation of the non-ideal samples could significantly improve the parametric response of the original "continuous", uncut sample. On the other hand, various physical mechanisms for post-fabrication dispersion correction are also available, as discussed later in this report.

In addition to difficult fabrication process, the characterization of high-confinement fibers such as HNLF poses significant challenge. Unfortunately, conventional dispersion measurement techniques are based on four wave mixing (FWM) and possess only sub-km spatial resolution. These were primarily designed to analyze fiber types such as conventional SMF or non-zero dispersion shifted fiber (DSF) , both having relatively high chromatic dispersion. For all methods, the longitudinal resolution has inverse dependence of measured dispersion. Intuitively, this is expected since the interacting frequency-separated waves create a feedback, an idler wave, which oscillates with spatial frequency proportional to fiber dispersion. In contrast, wideband parametric synthesis requires approximately meter-scale spatial resolution in nearly dispersion-less fiber such as HNLF, that has nearly a hundred-times lower dispersion than SMF in standard telecom band.

Consequently, this tutorial describes a class of non-destructive dispersion measurement techniques based on selective localization of FWM. Localization is achieved by means of counter-propagating pump pulse focused at certain position within the fiber span. The pump position is scanned to address all spatial points in a fiber.

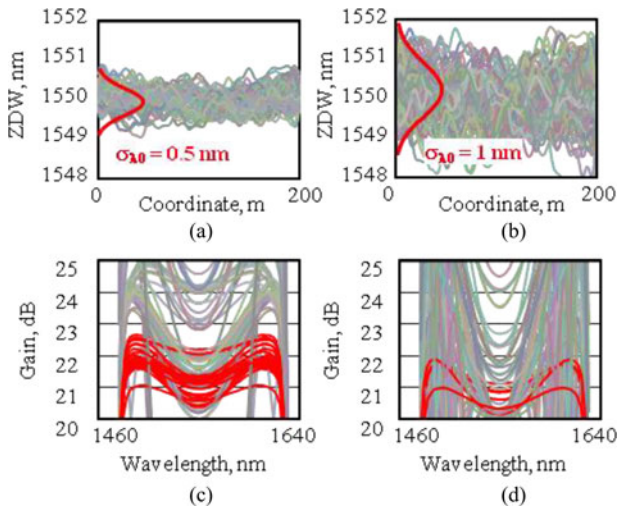

Fig. 1. Parametric gain spectral profile. Two realizations of ZDW map with standard deviation of $\sigma\lambda_0 = 0.5$ nm a) and $\sigma\lambda_0 = 1$ nm b). c) and d) are corresponding optimized parametric gain profiles. Minimum gain: 20 dB.

In Section II, we quantify the effects of dispersion fluctuations on the behavior of the practical device such as parametric amplifier. In Section III, we review the effectiveness of conventional measurement techniques. In Section IV, we describe the localization method. Underlying physics is discussed in Section V. An example of measurement architecture is given in Section VI. Performance considerations are discussed in Section VII. Measurement examples are presented in Section VIII. Finally, we estimate the impact of fluctuations in Section IX.

II. Effect of Dispersion Fluctuations to Parametric Gain

Sensitivity of the parametric gain to the variations of ZDW was investigated for a dual-pump phase insensitive parametric amplifier having a fiber with 200-m length, nonlinear coefficient of 20 /W/km, and dispersion slope of 0.025 ps/nm^2/km. The wavelength difference between the pumps was considered fixed and equal to 160 nm. Initially, 200 independent realizations of ZDW spatial profiles centered at $< \lambda_0 > = 1550$ nm were generated considering certain degree of correlation for ZDW values along spatial coordinate with characteristic correlation length of $L_C = 100$ m and two distinct values for the standard deviation $\sigma_{\lambda 0} = 0.5$ and 1 nm [26]. Unlike previously published results [25], [26] demonstrating parametric gains for fixed wavelengths and powers of the two pumps, we considered more realistic approach that includes certain optimization for the pump parameters. For each ZDW profile, the center frequency of the pumps and their powers were tuned in order to obtain the minimum gain of 20 dB and maximum flatness.

The simulation results are presented in Fig. 1. For $\sigma_{\lambda 0} = 0.5$ nm, the multiple realizations of the ZDW profile guaranty 3 dB flatness and minimum gain of 20 dB for sub-W pump powers. These "successful" realizations of the ZDW map are marked in red in Fig. 1(c) and (d). However, the sizable part of simulated ZDW profiles requires significant power

increase (>1 W) in order to compensate the gain at the central part of the spectrum. Such power increase is not desirable since an amplifier will require extra phase dithering stages for Brilloun suppression. For $\sigma_{\lambda 0} = 1$ nm, only few realizations satisfy target requirements, while the rest demonstrate significant gain variation across the spectrum exceeding 10 dB. The presented simulations verify a statement presented in the introduction section that a nanometer-scale control of the transversal geometry (or, equivalently, sub-nm variation of ZDW) is required in order to support high gain-bandwidth product.

III. Overview of the Existing Measuring Methods

The spatial mapping of the dispersion profile can be achieved by measuring response of the FWM process that depends on power and frequencies of the interacting waves (probes) and the local dispersion. If frequency-distinct co-propagating probes are injected into a fiber, they create idler waves that accumulate information about dispersion from the fiber input to a current spatial coordinate. If a physical gating mechanism extracting this information at any spatial position is provided, it is possible to obtain a full dispersion map. At the same time, the nondestructive requirement for the method dictates access only to fiber ends and cutting the fiber into pieces is not allowed.

The gating mechanisms can be separated into two main groups. For the first group, the localization is achieved "physically" at certain spatial (or corresponding temporal) position. Probes used in pulsed mode may be defined as the distinctive characteristic of this group. Alternatively, processing the spectral profiles of the idler waves corresponding to different frequencies of interacting probes (typically used in form of continuous waves) is the recognized property of the methods in the second group.

A technique presented in [27] relies on the fact that the two short pulses with different group velocities overlap within a certain walk-off interval that can be considered as physical resolution of the method. The resolution of several hundred of meters and accuracy of 0.2 nm for ZDW was demonstrated for DSF using 100-ps probes separated by 70 nm in wavelength. Such resolution is not sufficient for typical applications involving HNLFs. In [28] and [29], a more elegant OTDR-like solution demonstrating repeatable results was presented. The spatial gating was achieved by detecting the idler pulses back-reflected from different positions in a fiber. Unlike method described in [27], the OTDR method does not require extremely short pulses since back- reflection happens continuously at every spatial position and is not localized by the interval of pulse overlapping. In principle, arbitrary physical resolution (defined by a period of spatial oscillation and pulse duration) can be achieved. However, since the power efficiency of the FWM scaled inversely with the squared phase mismatch $\Delta\kappa$ ($\sim D \cdot \delta\lambda$), the power of the detected back-reflected idler becomes extremely low because only a little fraction of the generated idler is back-reflected. The described drawback was partly eliminated in [30] by adding a back-propagating probing wave interacting with the generated idler by means of stimulated Brillouin scattering (SBS).

A method presented in [31] and [32] and based on processing the FPM efficiencies of the two lasers synchronously tuned across ZDW can be attributed to the second group. The dispersion profile was extracted by solving an inverse problem. Specifically, the phase part of the conversion efficiency describing spatially varying dispersion was extracted from the measured amplitude (power) part using Fourier methods for phase reconstruction. The resolution of the scheme is defined by the addressed bandwidth that is proportional to the range over which one can acquire physically meaningful data. Considering typical parameters for HNLF and spacing between the probes of 50 nm, the meter-scale resolution can be achieved in theory. However, this method has a serious drawback: the spatial dispersion information is extracted from a convoluted amplitude profile that is potentially ambiguous since the "least informative" high power part of the measured response corresponds to the pump wavelengths passing ZDW, whereas the "detailed" part is concentrated on low-amplitude tails.

Finally, numerous publications (for example, [33]) demonstrating dispersion map reconstruction from the spectral profiles of the parametric gain corresponding different pump wavelengths were presented. Basically, the spatial dispersion function was optimized to fit the measured data. Unfortunately, these methods do not provide a physical interpretation of the spatial resolution. Worse, in small signal gain regime, the parametric response demonstrates reciprocal property [34]—the parametric gain profiles do not depend on the direction of propagation so that could not be related to a unique dispersion map.

IV. Description of Measuring Method

The idea of the introduced method is shown in Fig. 2 [35], [36]. Two probes pulses P_1 and P_2 with distinct frequencies f_1 and f_2 are launched into a fiber waveguide with sufficiently low powers to guarantee negligible nonlinear mixing. At certain position z_C, the power of one of the probes (P_1) is abruptly increased [see Fig. 2(b)], resulting in efficient probe mixing along the remaining fiber section [see Fig. 2(c)]. The localized power delivery was achieved by a pump pulse Π propagating in the opposite direction. The interaction between pulses happens during a short interval of pulse convolution. This switching interval represents the minimum spatial step (granularity) of the method, and thus defines the interval between two consecutive physically resolved measurements for the dispersion map. In practice, the length of the pulses is limited by the strength and the response time of the physical mechanism providing power transfer between the counter-propagating probe and pump. The collision position was progressively scanned along the fiber and powers of the FPM mixing product at frequency $(2f_1 - f_2)$ were collected at the fiber end. Consequently, the measured data provided unique signature of spatially distinct FPM process and were used to retrieve the spatial dispersion map of the entire fiber.

The SBS is an obvious mechanism for probe amplification. First of all, the strength of SBS is several orders of magnitude stronger than that of other $\chi^{(3)}$ nonlinear processes existing in nonlinear fibers such as Raman and Kerr [37]. This guaranties that the back-propagating pulse does not require significant power in order to provide certain gain, not exceeding 20 dB in practice, so that the pump pulse will not be distorted. The 10-ns response time of the SBS limits the minimum spatial

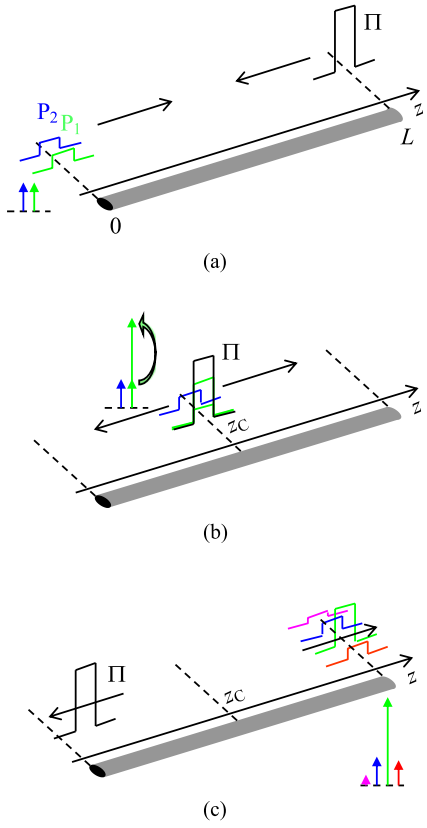

Fig. 2. Principle of dispersion measuring method: a) Two probes (P_1 and P_2) and a pump (Π) are launched to opposite ends of the fiber under test. b) At collision point z_C, a pump amplifies a probe P_1. c) At interval $[z_C, L]$ probes beat efficiently and generate FWM products.

duration of the pump pulse by meter, however, such resolution is even redundant for most applications utilizing nonlinear fibers. The estimation of the pump peak power for introduced dispersion scanner for typical HNLFs gives only few watts, unlike the alternative mechanism of stimulated Raman scattering that requires several hundreds of watts. The pulses with such high power do survive in a long fiber and typically generate the supercontinuum.

The narrow gain profile and the variation of the SBS spectral peak require precise locking between the pump and the probe center frequencies with precision equal to certain fraction of the SBS bandwidth [38]. In practice, the optimum Brillouin shift could vary along HNLF and has to be precisely matched along the entire length of the fiber in order to maintain maximum power transfer for each collision instance.

The SBS processes is polarization dependent—it happens that only one polarization state is preferentially amplified. Since the polarization state is not preserved in standard non-polarization maintaining (non-PM) fibers, but rather beats with certain characteristic length of meters comparable to typical pump pulse duration, so that the strict polarization alignment at each collision instance is required. The experiment demonstrated that the polarizations of *both* the probe and pump must be controlled to maximize the probe gain. This implies that their Stokes vectors must not only be co-aligned but also have a specific (linear, [39]) polarization state.

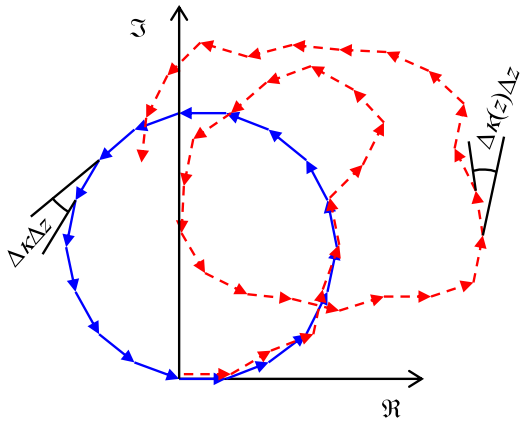

Fig. 3. Evolution of the idler vector amplitude in the phase space. Solid blue trajectory: constant dispersion $D = \text{const}$; dashed red trajectory: spatially-varying dispersion $D = D(z)$.

V. Physics of Measuring Method

The evolution of the generated FWM product can be represented by trajectories drawn by the end of the vector of the electric field $A_{\text{FWM}}(z)$ in phase space. The norm of this vector defines the optical power. In such representation, propagation along the fiber is equivalent to the vector sum of the elementary contributions defined by the left side of the equation

$$\frac{dA_{\text{FWM}}}{dz} = -j\gamma A_{P_1}^2(z)\, A_{P_2}(z)\, e^{j\Delta\varphi(z)} \tag{1}$$

in which A_{p1} and A_{p2} represent the complex envelopes of the probes, γ is a nonlinear coefficient, and $\Delta\varphi(z)$ is a sum of linear and nonlinear phase retardations experienced by the waves and accumulated between $z = 0$ and current coordinate z. In the simplified scenario of undepleted pumps, the total power of the idler measured at the end of the fiber is given by

$$P_{\text{FWM}}(L) = \eta\gamma^2 P_{P_1}^2 P_{P_2} L^2 \tag{2}$$

where a dimensionless factor η ($\eta < 1$) defines conversion efficiency. In such approximation, the modulation instability effect and the associated parametric gain were not considered.

If dispersion is constant across the whole fiber, the efficiency obtains "classical" sinc-type form given by

$$\eta = \left[\frac{\sin(\Delta\kappa L/2)}{\Delta\kappa L/2}\right]^2. \tag{3}$$

The formula for FWM conversion efficiency that includes attenuation is presented in [40] (Eq. (2)). In practice, the pump attenuation can be ignored for typical HNLF lengths of several hundred of meters. The propagation index mismatch $\Delta\kappa$ includes both linear (dispersion-dependent) and nonlinear (power-dependent) parts. In a vector space, the evolution of $A_{\text{FWM}}(z)$ happens along circular trajectory starting from the origin. It is clearly seen that, if a fiber length is sufficiently long, within some interval, the power is transferred from pumps toward the idler wave, then, a process reversed, as shown in Fig. 3. Such behavior is obvious since the elementary phasor $e^j\Delta\varphi$ at every interval Δz rotates at the same angle $\Delta\kappa\Delta z$ relatively to its

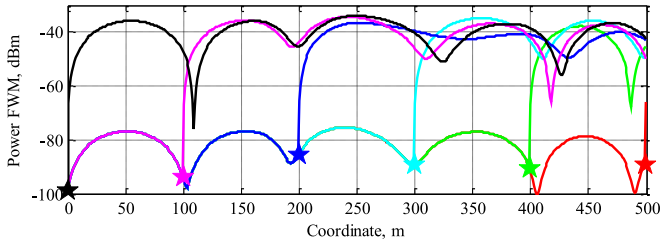

Fig. 4. Power evolution of the FWM product as a function of coordinate for different collision positions L_C (1, 100, 200, 300, 400, 499 m). Star-marker indicates a collision coordinate. Fiber length $L = 500$ m, gain $G = 20$ dB.

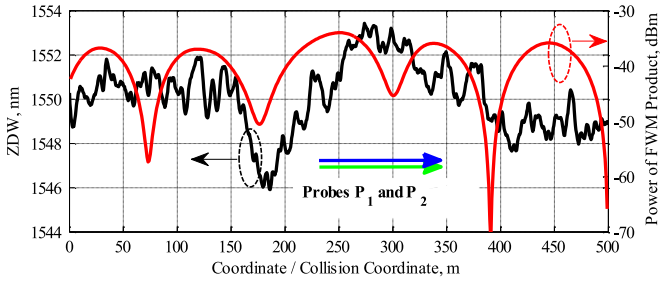

Fig. 5. Black curve: generated random dispersion profile as a function of spatial coordinate (left vertical axis); Red curve: simulated echo as a function of collision coordinate (right vertical axis). Two horizontal arrows point in the direction of probes' propagation.

previous orientation. In power domain, such evolution is equivalent to the periodic spatial power oscillations between zero and certain maximum value that is inversely proportional to the squared phase mismatch $\Delta\kappa$.

If dispersion is not stable along the fiber coordinate, the efficiency is represented by the complicated expression equal to the squared absolute value of the averaged phasor $e^{j\Delta\varphi(z)}$ with an argument $\Delta\varphi(z)$ equal to accumulated phase mismatch at coordinate z

$$\eta = \left|\frac{1}{L}\int_0^L e^{j\Delta\varphi(z)}dz\right|^2 = \left|\frac{1}{L}\int_0^L e^{j\int_0^z \Delta\kappa(z')dz'}dz\right|^2. \quad (4)$$

In this case, since the phase mismatch $\Delta\varphi$ is no longer a linear function: the end of the vector $A_{\mathrm{FWM}}(z)$ retraces some complicated spiral trajectory that does not necessarily returns to zero, as illustrated in Fig. 3. Correspondingly, the idler power demonstrates non-regular oscillations with coordinate-dependent periods and peaks.

The simulated example of idler evolution ($f_{\mathrm{FWM}} = 2f_{P1} - f_{P2}$) is shown in Fig. 4. First, a certain dispersion profile centered at 1550 nm was generated considering a correlated Gaussian random process [26] with 100-m correlation length and 1-nm standard deviation (black curve, Fig. 5). The power of the first probe at 1558 nm was 0 dBm, the power of the second probe offset by 2 THz (~1542 nm) was set to −10 dBm.

Probes propagated in a 500-m piece of fiber with dispersion slope of 0.04 ps/nm^2/km and nonlinear coefficient of 15 /W/km. At certain positions marked by stars in Fig. 4 and corresponding to collisions with backward-propagating pump, the first probe P_1 received 20 dB gain. It is clearly seen that, if collision happens

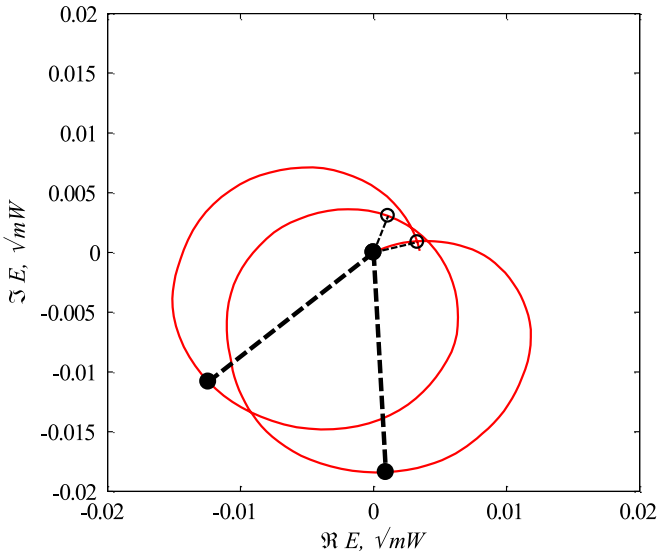

Fig. 6. Evolution of the FWM field amplitude in the complex space corresponding to collision coordinate $L_C = 300$ m. Filled black circles represent maximum powers ($z = 350$ and 450 nm), empty circles – minimum powers ($z = 410$ and 495 m).

at the end of the fiber, the idler power is practically negligible. For this case, at front section of the fiber (0–150 m), the average dispersion is relatively stable and the power shows smooth periodic behavior. Then, between 150 and 190 m, the ZDW drops by 4 nm and the period shortens since the rotation speed increases. Between 190 and 300-m, ZDW grows and period quickly increases since the spacing between the amplified probe and ZDW decreases.

By moving collision coordinate toward the beginning of fiber, the length of effective interaction increases. For every collision instance z_C, power of the idler demonstrates unique dependence $P_{\mathrm{FWM}}(z_C, z)$, thus ambiguity related to direction independence of the parametric gain [34] is resolved. The traces $P_{\mathrm{FWM}}(z_C = 0, z)$ and $P_{\mathrm{FWM}}(z_C = L, z)$ corresponding to collisions at both fiber ends are similar in shape but shifted vertically by roughly 40 dB, as predicted from Eq. (1). Some horizontal stretching of the trace is attributed to a certain amount of nonlinear rotation.

The obtained echo $P_{\mathrm{FWM}}(z_C)$ taken at the end of the fiber is shown in Fig. 5. It is clearly seen that the shape of the echo matches the evolution of the idler inside a fiber shown in Fig. 4 (black curve), but in reversed direction. This happens because the power of the idler is accumulated not from the beginning of the fiber but from the collision coordinate. The simulated evolution of the vector $A_{\mathrm{FWM}}(z)$ corresponding to 300-m collision coordinate of is shown in Fig. 6. Before collision, the power is low and marked by a green dot at the center; after collision, the vector makes two full rotations representing two periods shown in Fig. 4 (blue curve). For both rotations, a vector does not approach the origin so that the difference between minimum and maximum powers is finite (~10 dB).

VI. Experimental Setup

Fig. 7 illustrates the experimental setup constructed to validate the measuring principle. The output of the tunable CW

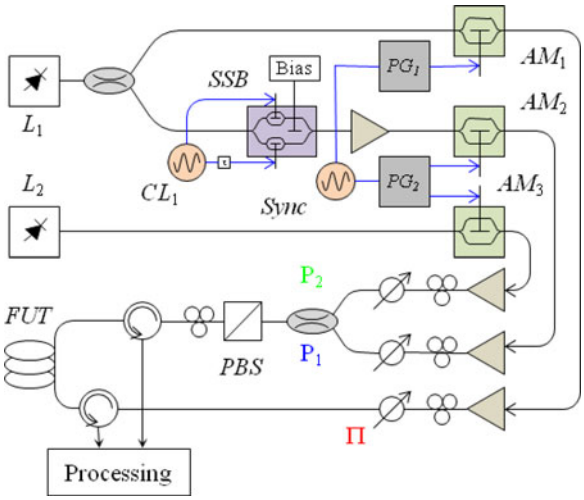

Fig. 7. Experimental setup.

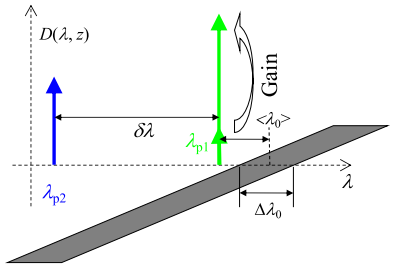

Fig. 8. Graphical interpretation of the probe spectral positioning providing both high sensitivity and spatial resolution.

laser L_1 was split to create the frequency-locked pump Π and the probe P_1 waves. The frequency of the probe wave was down-shifted by the exact Brillouin frequency (∼9.5 GHz for high-γ HNLFs at 1550 nm) using the single sideband modulator *SSB* driven by the adaptive clock CL_1. The clock tracked the exact Brillouin frequency for each collision instance. The shapes of the probe P_1 and pump pulses Π were created by the amplitude modulators AM_1 and AM_2. A second independent laser source L_2 and modulator AM_3 were used to generate a second probe P_2 co-propagating and overlapping with the probe P_1. The pump and probe pulses were generated by two independent pulse generators PG_1 and PG_2 synchronized to a master 100-KHz clock *Sync*. A set of amplifiers, filters, attenuators, and polarization controllers were used to manage the power and polarization states, and to suppress spontaneous noise. Circulators were used to couple counter-propagating pulses into a fiber under test *FUT* and to collect the response. Probes were launched through a polarizer *PBS* to ensure that two probes are co-polarized. Measurement process was fully automated requiring only initial manual collision localization at the very end of the fiber. The acquisition scheme contains a 1-nm filter separating an idler and a power meter. Strong polarization dependence of the SBS gain was resolved by placing the fast (∼10 KHz) polarization scrambler after a *PBS* so that the slow detector sees the polarization averaged, rather than the maximized, idler power. The alternative scheme with Faraday mirror providing precise polarization locking between the counter-propagating pulses was presented in Fig. 8 of [36]. In practice, a scheme shown in Fig. 7 provides better results since the Faraday mirror does not reverse the nonlinear polarization rotation experienced by a strong pump.

Before running a setup, the frequencies of interacting signals were precisely locked due to the excessively narrow peak (∼25 MHz) of the SBS gain profile. For this purpose, a clock was split and sent into two arms of the SSB modulator. The two "inner" biases were controlled by two commercial bias-stabilizing boards searching and holding the bias of the minimum transmission. The "outer" bias and 90° RF delay between modulator arms was set manually to achieve red-shift of the carrier, and to provide the maximum power for the downshifted sideband and minimum power for any other harmonic by observing the OSA spectrum. By proper alignment, the original carrier can be fully eliminated (>30 dB), and blue-shifted harmonic can be suppressed by more than 20 dB.

Secondly, the extinction ratio of the pump and probe pulses must be maximized to avoid relatively strong SBS interaction of the probe with long pump pedestal. In practice, this effect causes significant degradation of the measuring contrast (ratio of maximum and minimum powers P_{FWM}) since the pump-probe interactions spread over the whole fiber and become no longer localized. This problem was resolved by precise setting for the bias of the modulator AM_1 for the collision that happens outside the fiber but close to the fiber input. In this case, even millivolt offset from the optimum (i.e. minimum gain) bias caused observable probe amplification.

VII. Spatial Resolution Considerations

The spatial resolution and the accuracy of the dispersion (or ZDW) characterization are two effective parameters that define the application limits of the presented method, as well as the limits for the methods described in [27]–[32]. Since information about spatial dispersion map is extracted from the multiple measurements of the power of FWM product continuously gated along the fiber coordinate, these two resolution parameters are correlated and could not be fully decoupled. This statement is rather obvious since the information about dispersion is imprinted to both "vertical" coordinate representing power, and "horizontal" coordinate defining specific spatial pattern of the power profile. Careful analysis of the Eq. (2)–(4) shows that the vertical and horizontal metrics demonstrates different sensitivity to dispersion variation. Specifically, the speed of the spatial oscillation scaled linearly with the phase mismatch ($\Delta\kappa \sim D$), whereas the power of the idler wave decreases as a quadratic function. This implies that the resolution of the method based on measuring of FWM interactions could not be programmed to infinitely small value since the detected power could quickly drop below a certain threshold, typically limited by the detector thermal noise. On the other hand, the accuracy of the measured dispersion is directly related to signal-to-noise ratio (SNR) of the measured echo (P_{FWM}). To increase SNR, the powers of the probes should be increased, but the effects related to nonlinear phase rotation start playing role. In this case, the complexity of

the dispersion recovery algorithm significantly increases since the linear and nonlinear rotations should be separated. In such a case, this algorithm requires measuring the nonlinear coefficient ([41], [42]) and knowledge of the precise evolution of the probes inside a fiber.

The methods for dispersion recovery are described in detail in ref. [35] and [36]. In short terms, in order to get spatial resolution equal to duration of the pump-prove interaction (meter-scale) and precision of ZDW below 0.1 nm, the entire set of powers $P_{\mathrm{FWM}}(z_C)$ should be measured with extremely high precision not exceeding 0.1 dB. Such experimental precision is very problematic since *a*) the gain is polarization dependent and, *b*) in typical HNLFs, the linear rotation is not regular and often happens faster than the spatial duration of the pulses. The polarization effect causes small probe power oscillations for closely spaced collisions and could not be separated from noise-related oscillations. In practice, 10-m spatial resolution is sufficient for applications requiring HNLFs with lengths of several hundred meters, so that the described "advanced" analysis is not needed. Indeed, if the period of spatial oscillation approaches several meters, it roughly defines the resolution, no matter which power is detected. In this case, the precise "vertical" information is simply redundant—the only condition that must be satisfied: the power of the idler is sufficient to resolve the localized periods. In practice, the average power of -60 dBm of the pulsed idler can be easily detected with sufficient SNR by a slow photo-detector.

The accuracy of the modified counter-colliding method requires special considerations with respect to probe/ZDW and probe P_1/probe P_2 spectral positioning. Firstly, the period of the complete spatial oscillation Λ_z roughly given by

$$\int_{z}^{z+\Lambda_z} \Delta\kappa\,(z)\,dz = \langle \Delta\kappa\,(z, z+\Lambda_z)\rangle\,\Lambda_z = 2\pi \qquad (5)$$

defines the *resolution*. $<\Delta\kappa(z)>$ is the averaged propagation index mismatch at interval $(z, z+\Lambda_z)$ given by [28]

$$f_{\mathrm{Z}} = \frac{1}{\Lambda_{\mathrm{Z}}} = \frac{\langle\Delta\kappa\rangle}{2\pi} = cS\,(\lambda_{\mathrm{P}_1} - \lambda_0\,(z))\left(\frac{\delta\lambda}{\lambda}\right)^2 \qquad (6)$$

in which S is a fiber dispersion slope, c is speed of light, $\delta\lambda = \lambda_{P1} - \lambda_{P2}$ is the wavelength spacing between the probes.

However, the resolution itself is not sufficient since it is related to dispersion/ZDW accuracy, as mentioned before. It is important to predict the sensitivity of the method to the variation of the ZDW. As an illustration, let us consider the following example: assume that ZDW between two nearest resolved coordinates in the typical HNLF with dispersion slope of 0.03 ps/nm^2/km changes from 1550 to 1551 nm. According to Eq. (6), if we select wavelengths of the probes separated by 25 nm, in order to get 10-m spatial resolution, the center frequency of the probes should be shifted toward 1510 nm. At the same time, the period of the spatial oscillation will change by only 25-cm, which is comparable to the accuracy of positioning of localized power delivery roughly equal to 1 m. This simple calculation states that, in such configuration (a pair of frequencies $f_{\mathrm{P}1}$ and $f_{\mathrm{P}2}$), the spatial sensitivity of the method is not sufficient to resolve such sizable ZDW change of 1 nm.

The accurate consideration is the following: let us consider that the spatial frequency at two resolved coordinates z_1 and z_2 are $f_z(z_1)$ and $f_z(z_2)$. Their normalized difference ξ (or a contrast factor) can be directly obtained from Eq. (6) and is given by

$$\xi = \frac{f_z\,(z_1) - f_z\,(z_2)}{1/2\,(f_z\,(z_1) + f_z\,(z_2))} = \frac{\Delta\lambda_0\,(z_1, z_2)}{\lambda_{\mathrm{P}_1} - \langle\lambda_0\rangle}. \qquad (7)$$

This parameter defined the dynamic range of the spatial resolution. At best-case scenario, even small change of ZDW between two resolved spatial positions should significantly modify this factor. As seen from Eq. (7), in order to maximize ξ, (i.e. in order to increase the sensitivity), the denominator has to be minimized since the measured $\Delta\lambda_0$ is a given parameter of FUT. Consequently, this means that the position of the probe wavelength should be set closely to the averaged (global) ZDW, or equivalently, the predicted deviation of ZDW should be a sizable part of the spacing between the wavelength of the probe P_1 and the average ZDW. In other words, the spacing between the amplified probe and average ZDW defines the sensitivity of the method, whereas the spacing between the probes P_1 and P_2 $\delta\lambda$ defines the spatial resolution (Eq. (6)). In practice, the contrast ξ of 50% is a readily attainable choice. In case if ZDW variations are too high (>5 nm), the best strategy is to scan FUT using several different probe wavelengths λ_1 and λ_2, and then, combine multiple measurements. All written above is summarized in Fig. 8. The illustrative example for the estimation of the probe wavelengths is provided in [36].

VIII. Experimental Results

A. Polarization Maintaining HNLF

The efficiency of the parametric interactions between signals and pumps are strongly dependent on their polarization alignment. In this sense, polarization maintaining operation of HNLF-based devices is a preferable regime, providing stable parametric response and not requiring permanent polarization tracking or complicated polarization insensitive schemes [43]. In order to map dispersion of such fiber, a scheme shown in Fig. 7 should be modified: the standard non-PM passive circulators should be replaced by PM versions. The resulted measured echo corresponding to slow and fast axes of the elliptic-core PM-HNLF with dispersion slope of 0.027 ps/nm^2/km and nonlinear coefficient of 10 /W/km are shown Fig. 9. The dispersion profiles reconstructed with 5–10-m spatial resolution are shown in Fig. 10. The average ZDWs for two orthogonal axes differ by 45 nm.

First or all, the oscillations mapping the dispersion properties are not regular but change along the fiber. Second: one should pay attention that the oscillations for both axes are correlated—peaks and valleys of the dispersion maps approximately match. In order to verify that the measured dispersion maps are real, the fiber was scanned using noise injection technique [45]. The narrow-band amplified noise was tuned across ZDW. The noise beat with the second CW probe widely separated in wavelength. The sharp and narrow peak of the generated idler indicates stable dispersion characteristic whereas the wide low-power idler spectrum indicates significant deviation of the ZDW. Half

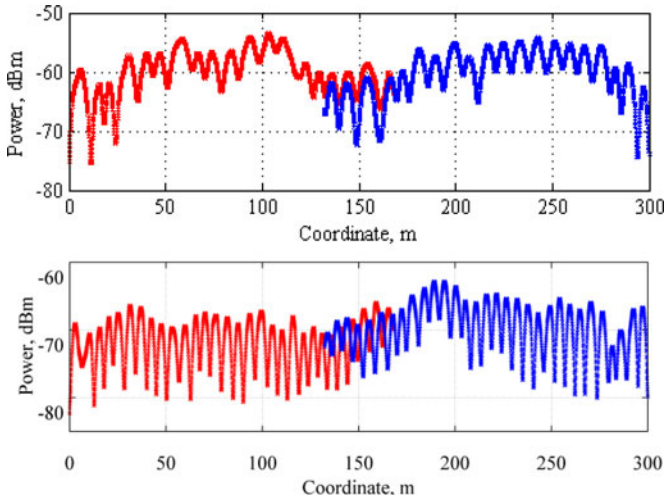

Fig. 9. Measured echo for slow ($\lambda_{P1} = 1530$ nm, $\lambda_{P2} = 1580$ nm) (top); and fast ($\lambda_{P1} = 1560$ nm, $\lambda_{P2} = 1600$ nm) (bottom) polarization axes. Pulse length: 2 m, scanning step: 10 cm.

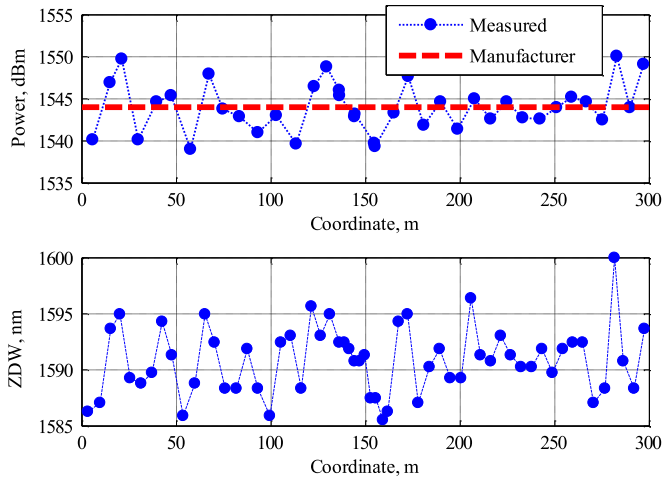

Fig. 10. Reconstructed ZDW for slow (top) and fast (bottom) polarization axes. Red dashed line indicates ZDW provided by a manufacturer. Circles indicate centers of the oscillation period.

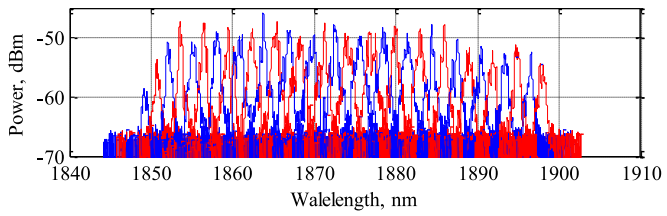

Fig. 11. Spectrum of the idler measured using noise injection method. Noise center wavelength: 1533.5, 1534.0 . . . 1550 nm, probe wavelength: 1310 nm.

of the width of the idler spectrum is roughly equal to ZDW deviation. The spectra measured for the slow axis are shown in Fig. 11. It is clearly seen that the spectrum spreads over more than 30 nm and matches with the maximum ZDW deviation shown in Fig. 10.

B. Short Standard "Sloped" HNLF

The second example demonstrates that the power of the probe pulse can be set quite freely. Fig. 12 shows maps of idler oscillations and retrieved ZDW corresponding to the two probes different in power by 7 dB. It is clearly seen that the periods of the FWM oscillations are preserved because the main contribution to the phase mismatch $\Delta\varphi$ (Eq. 1) is formed by the linear dispersive term.

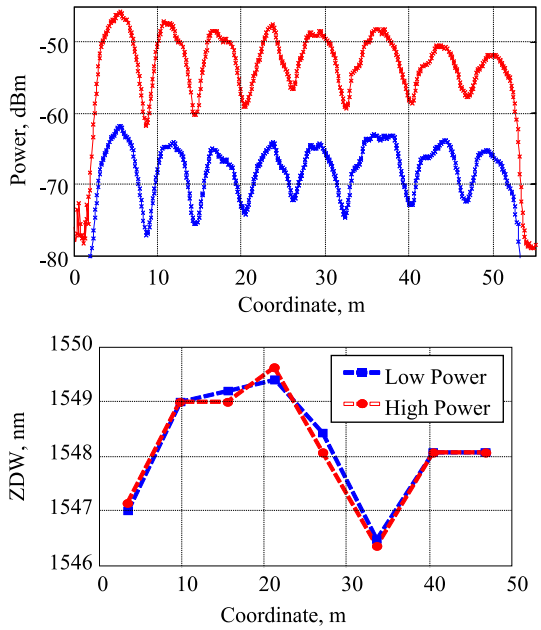

Fig. 12. Top: Measured echo as a function of collision coordinate. Pulse length: 2 m, scanning step: 10 cm, probe wavelength $\lambda_1 = 1537$ nm, second pulse wavelength: $\lambda_2 = 1608$ nm, dispersion slope S: 0.024 ps/nm^2/km. Bottom; reconstructed map of ZDW.

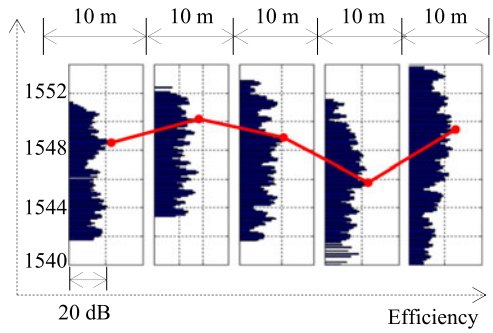

Fig. 13. Measured efficiency as a function of noise center wavelength. Unlike Fig. 11, the spectra are shifted toward the center frequency of the probe represented by a filtered noise source. Wavelength of the second probe: 1310 nm.

The fiber was cut into five 10-m-long pieces and each piece was scanned using the noise injection method. The measured spectra of the idler are shown in Fig. 13. It is seen that idler spectra are not resonant even for short pieces. This measurement implies that there are different scales of the ZDW fluctuations: *a*) the short-length sub-meter scale, and *b*) long scale (1–10 m), as predicted in [44]. The solid red line connects peak efficiencies corresponding to each 10-m section and matches quite well with the averaged ZDW demonstrated in Fig. 13.

Multiple examples of the measured ZDW profiles for "standard" 200–300-m-long pieces for both C and L-band fibers are demonstrated in [36] and [52].

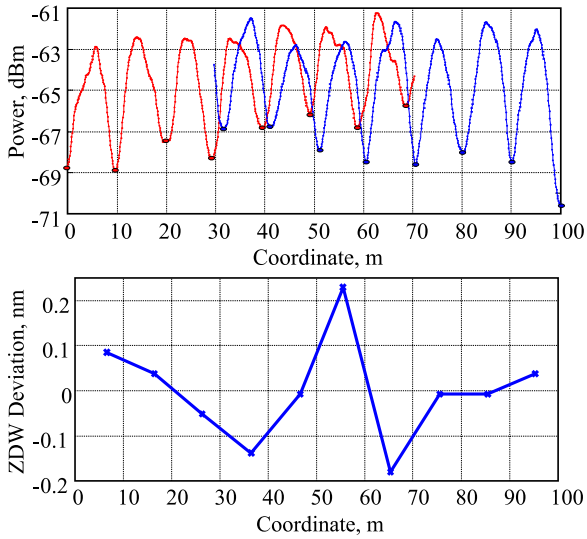

Fig. 14. Top: Measured power of FWM product as a function of collision coordinate. Pulse length: 4 m, scanning step: 10 cm, probe wavelength $\lambda_1 = 1560.582$ nm, second pulse wavelength: $\lambda_2 = 1610$ nm, dispersion slope S: 0.079 ps/nm^2/km. Bottom: ZDW map reconstructed from data measured in both directions. ZDW deviation is specified relatively average $\lambda_0 = 1565.1$ nm.

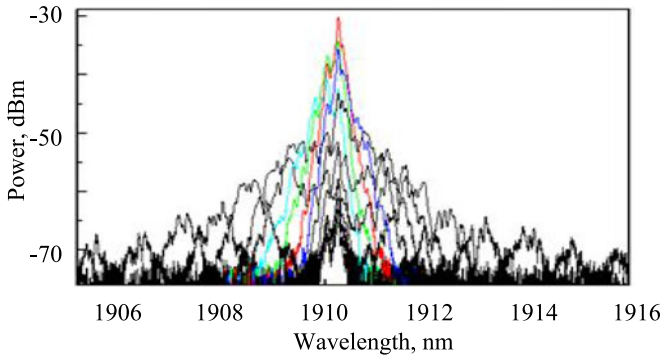

Fig. 15. Measured conversion spectra for different noise center wavelength. Wavelength of the second probe: 1288.48 nm.

C. Dispersion Shifted Fiber

The method was applied to scan ZDW map of the fiber types other than HNLF. Fig. 14 demonstrates the nonlinear echo generated in a 100-m-long sample of the DSF. The 10-m oscillations are regular across the whole fiber indicating extremely low variations of ZDW. The 4-m duration of the probe and pump pulses was used because of relatively low nonlinearity ($\gamma = 2.5$ /W/km) of the DSF. The dispersion map was verified by the method of amplified noise. Fig. 15 shows that the resonant structure of the parametric response verifying ultra-low dispersion drift.

D. Dispersion-Stabilized HNLF

The nonlinear fibers possessing spatially stable dispersion were recently introduced [46], [47]. Such outstanding fiber property was achieved by special design of the transversal refractive index profile. Importance of the new HNLF was motivated by needs effective suppression of the SBS since the typical applications require CW pump powers significantly exceeding SBS threshold. Stable ZDW is also required in order to achieve effective distant (few hundreds of nanometer) conversion driven by the negative forth order dispersion [48]. It was demonstrated that the original dispersion fluctuations were preserved even if varying tensile stress was applied to HNLF in order to suppress SBS. In optical parametric oscillators, the new fiber design provides benefits over conventional DSF, requiring significantly lower emission threshold and, correspondingly, higher efficiency [46], [47].

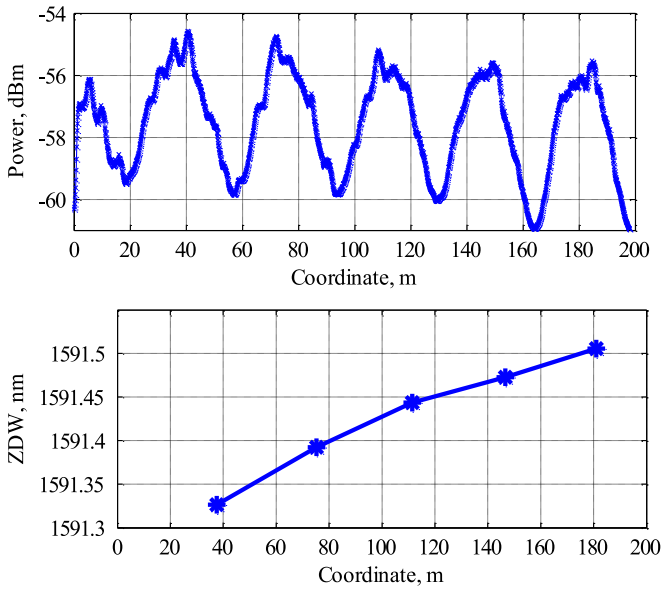

Fig. 16. Top: Measured echo as a function of collision coordinate. Pulse length: 2 m, scanning step: 10 cm, probe wavelength $\lambda_1 = 1542$ nm, second pulse wavelength: $\lambda_2 = 1590$ nm, dispersion slope S: 0.067 ps/nm^2/km. Bottom: Reconstructed map of ZDW.

The 200-m-long L-band dispersion-stabilized HNLF with nonlinear coefficient of 8 /W/km and dispersion slope of 0.067 ps/nm^2/km was characterized using a method of the counter-colliding pulses. The measured echo is shown in Fig. 16. Similar to DSF, the spatial power oscillations of the idler are stable over the whole fiber length reflecting extremely low ZDW fluctuations of 0.15 nm.

E. Dispersion-Flattened HNLF (DF-HNLF)

Finally, the introduced method was applied in order to calibrate the dispersion properties of the DF-HNLFs. The typical applications requiring DF-HNLFs such as parametric comb generators require ultra-stable dispersion profile with variation not exceeding 0.1 ps/nm/km [24]. The algorithm of the dispersion reconstruction and an example of the measured ZDW map in a fiber with significant dispersion fluctuation were presented in [49]. Unlike conventional sloped fibers, the calibration procedure for ZDW requires knowledge of the forth order dispersion coefficient β_4 defining curvature of the dispersion profile. Since the forth order dispersion coefficient is typically considered as a stable parameter, it can be estimated from averaged (non-localized) dispersion profile of the long (>100 m) sample obtained using conventional dispersion analyzer. In a short piece (~1 m) of DF-HNLF, β_4 can be accurately predicted using an interferometric method described in [50]. Fig. 17 shows

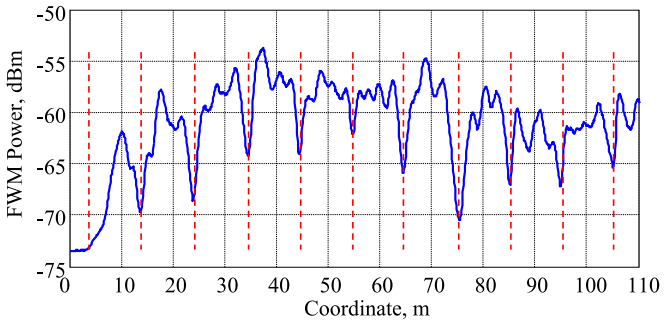

Fig. 17. Measured echo as a function of collision coordinate. Pulse length: 2 m, scanning step: 10 cm, probe wavelength $\lambda_1 = 1545$ nm, second pulse wavelength: $\lambda_2 = 1599$ nm.

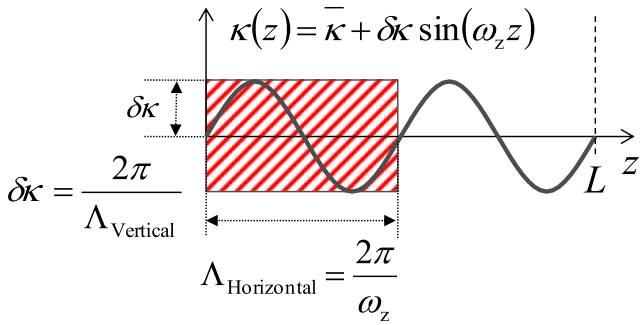

Fig. 18. Graphical representation of the characteristic scales of dispersion variations. $\kappa(z)$ is the propagation index mismatch. $\Lambda_{\text{Horizontal}}$ is a period of spatial oscillation of ZDW, $\Lambda_{\text{Vertical}}$ is associated with the ZDW fluctuation amplitude.

measured echo in a 110-m long fiber with stable oscillation pattern. The high frequency oscillations modulating main pattern mapping dispersion fluctuations are related to incomplete polarization mixing since, in typical DF-HNLFs, polarization rotates in meter and sub-meter scale. Precise calibration described in [49] predicts variation of the peak of dispersion profile of below 0.02 ps/nm/km and negative dispersion peak of -0.15 ps/nm/km. This fiber was used as the last stage of the comb source spanning over 120 nm demonstrated in [20].

IX. Dispersion Fluctuations: Discussion

The results presented in previous section show that the dispersion fluctuations of the certain fiber types could be quite significant. In fact, these fiber types (high-γ HNLF and DF-HNLF) are mostly needed in practice, since the fibers with stabilized dispersion are designed for specific purposes such as distant parametric converters and OPO [47], [48]. Multiple measurements demonstrated that the recently fabricated high-γ HNLFs ($\gamma > 20$ /W/km) possess more than 1-nm ZDW fluctuations (at best) over typical 100-m-long samples. The fluctuations in the HNLFs fabricated a decade ago are even more significant, as well as the fluctuations in PM-HNLFs shown in Fig. 10. At first glance, this result states that such fibers are defective and could not be used as a nonlinear mixer. However, it is not fully true since the parametric response depend significantly of the form of the dispersion fluctuation [25]. If one considers a specific simplified case of periodic sinusoidal dispersion fluctuation drawn in Fig. 18, one can show that the parametric gain g can be represented by the following formula:

$$g^2 = \left(\bar{g}^2 + \frac{1}{\Lambda_{\text{Vertical}}\Lambda_{\text{Horizontal}}}\{\cdots\} + \frac{1}{\Lambda_{\text{Vertical}}\Lambda_{\text{NL}}}\{\cdots\}\right) \tag{8}$$

in which $\bar{g}^2$ is the gain associated with the average dispersion profile represented the linear phase mismatch $\bar{\kappa}$. Physical sense of the characteristic lengths defining dispersion variations is clear from Fig. 18, $L_{\text{NL}} = 1/\gamma P$ is a nonlinear characteristic length. The terms in brackets $\{\ldots\}$ modulating the parametric gain profile and containing to periodic functions of $\omega_z z$ are not shown in Eq. 8. These terms define the degradation of the gain flatness and can be suppressed by decreasing the area of the rectangle ($\Lambda_{\text{Horiziontal}}\Lambda_{\text{Vertical}}$) circumscribing a single period of dispersion fluctuation, as shown in Fig. 18. Strictly speaking, the slow and low amplitude variations of ZDW are washed out in the nonlinear process. Vise versa, the slow high-amplitude monotonic variations have significant impact on the parametric gain flatness. This idea can be applied to "stabilize" gain profile, making it immune to variations of ZDW. If the ZDW map is precisely measured, the worst fiber sections having large variations (i.e. large $\Lambda_{\text{Vertical}}$) of ZDW can be cut out. At the same time, the fast spatial oscillations of ZDW can be artificially induced by concatenating sections of the fiber having largest variations opposite in sign (i.e. decreasing $\Lambda_{\text{Horiziontal}}$), while keeping average ZDW approximately constant along the fiber [51].

The measurements of the dispersion properties of strained HNLFs have indicated that its ZDW shifts to a red side of the spectrum as the applied tension increases, also demonstrating linear dependence. Specifically, it was found that ZDW can be shifted in excess of 10 nm before the tension approaches fiber breaking limit of several kilograms. This property can be used to eliminate the HNLF dispersive fluctuations: a spooler with electronically controlled tension programmed in accordance to the measured spatial ZDW profile can simply invert the fluctuation map. The example of such technique was demonstrated in [52].

It is important to note that the fluctuations in dispersion profile of the fiber can also be compensated by a variety of other means that include, but are not limited to photorefractive index tailoring, heat treatment and electro-optical effects. All these mechanisms require precise, prior knowledge of dispersive fluctuation map before their applications.

X. Conclusion

A family of measurement techniques for non-destructive mapping of fiber dispersion was described. The theoretical basis, underlying physics, and implementation was discussed along with its limits. We illustrate the technique on examples of different fiber types such as silica highly nonlinear HNLFs, dispersion-flattened, and dispersion-stabilized HNLFs. The spatial (longitudinal) resolution and the dynamic range (sensitivity) of the method can be programmed, allowing the general principle to be applied to a wide variety of fiber types and nonlinear devices. The spatial resolution of several meters and the resolution of ZDW below 0.1 nm have been achieved.

REFERENCES

[1] R. H. Stolen, "The early years of fiber nonlinear optics," *J. Lightw. Technol.*, vol. 26, no. 9, pp. 1021–1031, May 1, 2008.

[2] J. M. Dudley and J. R. Taylor, "Ten years of nonlinear optics in photonic crystal fibre," *Nature Photon.*, vol. 3, pp. 85–90, 2009.

[3] G. Agrawal, *Applications of Nonlinear Fiber Optics*. New York, NY, USA: Academic, 2008.

[4] S. A. Akhmanov, V. A. Vysloukh, A. S. Chirkin, *Optics of Femtosecond Laser Pulses*. College Park, MD, USA: Amer. Inst. Phys., 1992.

[5] T. Torounidis, P. A. Andrekson, and B. Olsson, "Fiber-optical parametric amplifier with 70-dB gain," *IEEE Photon. Technol. Lett.*, vol. 18, no. 10, pp. 1194–1196, May 15, 2006.

[6] R. H. Stolen and J. E. Bjorkholm, "Parametric amplification and frequency conversion in optical fibers," *IEEE J. Quantum Electron.*, vol. QE-18, no. 7, pp. 1062–1072, Jul. 1982.

[7] M. Hirano *et al.*, "Silica-based highly nonlinear fibers and their application," *IEEE J. Sel. Topics Quantum Electron.*, vol. 15, no. 1, pp. 103–113, Jan. 2009.

[8] Corning SMF-28e +Optical Fiber, Product Information. URL: http://www.corning.com/opticalfiber/products/SMF-28e+_fiber.aspx

[9] P. S. Andre and A. N. Pinto, "Chromatic dispersion fluctuations in optical fibers due to temperature and its effects in high-speed optical communication systems," *Opt. Commun.*, vol. 246, pp. 303–311, 2005.

[10] S. Radic and C. J. McKinstrie, "Two-pump fiber parametric amplifiers," *Opt. Fiber Technol.*, no. 9, pp. 7–23, 2003.

[11] S. Watanabe, S. Takeda, and T. Chikama, "Interband wavelength conversion of 320 Gb/s (32 × 10 Gb/s) WDM signal using a polarization-insensitive fiber four-wave mixer," in *Proc. Eur. Cong Opt. Commun.*, 1998, vol. 3. pp. 83–87.

[12] B. P. Kuo, E. Myslivets, N. Alic, and S. Radic, "Wavelength multicasting via frequency comb generation in a bandwidth-enhanced fiber optical parametric mixer," *J. Lightw. Technol.*, vol. 29, no. 23, pp. 3515–3522, Dec. 1, 2011.

[13] C.-S. Brès, "Wavelength multicasting of 320-gb/s channel in self-seeded parametric amplifier," *IEEE Photon. Technol. Lett.*, vol. 21, no. 14, pp. 1002–1005, Jul. 15, 2009.

[14] R. Slavík, F. Parmigiani, J. Kakande, C. Lundstrm, M. Sjdin, P. A. Andrekson, R. Weerasuriya, S. Sygletos, A. D. Ellis, L. Grner-Nielsen, D. Jakobsen, S. Herstrm, R. Phelan, J. O'Gorman, A. Bogris, D. Syvridis, S. Dasgupta, P. Petropoulos, and D. J. Richardson, "All-optical phase and amplitude regenerator for next-generation telecommunications systems," *Nature Photon.*, vol. 4, pp. 690–695, 2010.

[15] F. Parmigiani, C. Finot, K. Mukasa, M. Ibsen, M. A. F. Roelens, P. Petropoulos, and D. J. Richardson, "Ultra-flat SPM-broadened spectra in a highly nonlinear fiber using parabolic pulses formed in a fiber Bragg grating," *Opt. Exp.*, vol. 14, no. 17, pp. 7617–7622, 2006.

[16] G. Berrettini, G. Meloni, A. Bogoni, and L. Poti, "All-optical 2×2 switch based on Kerr effect in highly nonlinear fiber for ultrafast applications," *IEEE Photon. Technol. Lett*., vol. 18, no. 23, pp. 2439–2441, Dec. 1, 2006.

[17] B. P.-P. Kuo, E. Myslivets, A. O. J. Wiberg, S. Zlatanovic, C.-S. Brés, S. Moro, F. Gholami, A. Peric, N. Alic, and S. Radic, "Transmission of 640-Gb/s RZ-OOK channel over 100-km SSMF by wavelength-transparent conjugation," *J. Lightw. Technol.*, vol. 29, no. 4, pp. 516–523, Feb. 15, 2011.

[18] P. A. Andrekson, H. Sunnerud, S. Oda, T. Nishitani, and J. Yang, "Ultrafast, atto-joule switch using fiber-optic parametric amplifier operated in saturation," *Opt. Exp.*, vol. 16, no. 15, pp. 10956–10961, 2008.

[19] P. A. Andrekson and M. Westlund, "Nonlinear optical fiber based high resolution all-optical waveform sampling," *Laser Photon. Rev.*, vol. 1, no. 3, pp. 231–248, 2007.

[20] E. Temprana, V. Ataie, B. P.-P. Kuo, E. Myslivets, N. Alic, and S. Radic, "Low-noise parametric frequency comb for continuous C-plus-L-band 16-QAM channels generation," *Opt. Exp.*, vol. 22, no. 6, pp. 6822–6828, 2014.

[21] T. Okuno, M. Hirano, T. Nakanishi, and M. Onishi, "Highly-nonlinear optical fibers and their applications," *SEI Tech. Rev.*, no. 62, pp. 34–40, 2006.

[22] K. Igarashi, H. Tobioka, S. Kuroki, R. Miyabe, J. Hiroishi, M. Takahashi, T. Yagi, O. Aso, and S. Namiki, "A highly nonlinear fiber module and its application to the generation of ultra-high repetition-rate sub-picosecond optical pulse trains," *Furukawa Rev.*, no. 25, pp. 9–12, 2004.

[23] D. A. Chestnut and J. R. Taylor, "Soliton self-frequency shift in highly nonlinear fiber with extension by external raman pumping," *Opt. Lett.*, vol. 28, no. 24, pp. 2512–2514, 2003.

[24] E. Myslivets, B. P. P. Kuo, N. Alic, and S. Radic, "Generation of wideband frequency combs by continuous-wave seeding of multistage mixers with synthesized dispersion," *Opt. Exp.*, vol. 20, no. 3, pp. 331–3344, 2012.

[25] F. Yaman, Q. Lin, S. Radic, and G. P. Agrawal, "Impact of dispersion fluctuations on dual-pump fiber-optic parametric amplifiers," *IEEE Photon. Technol. Lett.*, vol. 16, no. 5, pp. 1292–1294, May 2004.

[26] M. Farahmand and M. de Sterke, "Parametric amplification in presence of dispersion fluctuations," *Opt. Exp.*, vol. 12, pp. 136–142, 2004.

[27] M. Eiselt, R. M. Jopson, and R. H. Stolen, "Nondestructive position resolved measurement of the zero-dispersion wavelength in an optical fiber," *J. Lightw. Technol.*, vol. 15, no. 1, pp. 135–143, Jan. 1997.

[28] L. F. Mollenauer, P. V. Mamyshev, and M. J. Neubelt, "Method for facile and accurate measurement of optical fiber dispersion maps," *Opt. Lett.*, vol. 21, no. 21, pp. 1724–1726, 1996.

[29] J. Gripp and L. F. Mollenauer, "Enhanced range for OTDR-like dispersion map measurements," *Opt. Lett.*, vol. 23, no. 20, pp. 1603–1605, 1998.

[30] K.-Y. Song, M. G. Herráez, and L. Thévenaz, " Mapping of chromatic-dispersion distribution along optical fibers with 20-m spatial resolution," *J. Lightw. Technol.*, vol. 23, no. 12, pp. 4140–4146, Dec. 2005.

[31] I. Brener, P. P. Mitra, D. D. Lee, D. J. Thomson, and D. L. Philen, "High-resolution zero-dispersion wavelength mapping in single-mode fiber," *Opt. Lett.*, vol. 23, no. 19, pp. 1520–1522, 1998.

[32] M. González-Herráez, P. Corredera, M. L. Hernanz, and J. A. Méndez, "Retrieval of the zero-dispersion wavelength map of an optical fiber from measurement of its continuous-wave four-wave mixing efficiency," *Opt. Lett.*, vol. 27, no. 17, pp. 1546–1548, 2002.

[33] A. Mussot, E. Lantz, A. Durécu-Legrand, C. Simonneau, D. Bayart, T. Sylvestre, and H. Maillotte, "Zero-dispersion wavelength mapping in short single-mode optical fibers using parametric amplification," *IEEE Photon. Technol. Lett.*, vol. 18, no. 1, pp. 22–24, Jan. 1, 2006.

[34] M. E. Marhic, G. Kalogerakis, and L. G. Kazovsky, "Gain reciprocity in fiber optical parametric amplifiers," *Electron. Lett.*, vol. 42, no. 9, pp. 519–520, 2006.

[35] E. Myslivets, N. Alic, J. R. Windmiller, and S. Radic, "A new class of high-resolution measurements of arbitrary-dispersion fibers: Localization of four-photon mixing process," *J. Lightw. Technol.*, vol. 27, no. 3, pp. 364–375, Feb. 1, 2009.

[36] E. Myslivets, N. Alic, and S. Radic, "High resolution measurement of arbitrary-dispersion fibers: Dispersion map reconstruction techniques," *J. Lightw. Technol.*, vol. 28, no. 23, pp. 3478–3487, Dec. 1, 2010.

[37] R. G. Smith, "Optical power handling capacity of low loss optical fibers as determined by stimulated raman and brillouin scattering," *Appl. Opt.*, vol. 11, no. 11, pp. 2489–2494, 1972.

[38] M. Nikles, L. Thevenaz, and P. A. Robert, "Brillouin gain spectrum characterization in single-mode optical fibers," *J. Lightw. Technol.*, vol. 15, no. 10, pp. 1842–1851, Oct. 1997.

[39] M. Oskar van Deventer and A. J. Boot, "Polarization properties of stimulated brillouin scattering in single-mode fibers," *J. Lightw. Technol.*, vol. 12, no. 4, pp. 585–590, Apr. 1994.

[40] K. Inoue, "Four-wave mixing in an optical fiber in the zero-dispersion wavelength region," *J. Lightw. Technol.*, vol. 10, no. 11, pp. 1553–1561, Nov. 1992.

[41] A. Boskovic, S. V. Chernikov, J. R. Taylor, L. Grüner-Nielsen, and O. A. Levring, "Direct continuous-wave measurement of n_2 in various types of telecommunication fiber at 1.55 mm," *Opt. Lett.*, vol. 21, no. 24, pp. 1966–1968, 1996.

[42] C. Vinegoni, M. Wegmuller, and N. Gisin, "Determination of nonlinear coefficient n_2/Aeff using self-aligned interferometer and faraday mirror," *Electron. Lett.*, vol. 36, no. 10, pp. 886–888, 2000.

[43] L. Gruner-Nielsen, Polarization maintaining highly nonlinear fibers and their applications," in *Proc. IEEE/LEOS Winter Top. Meeting*, 2009, pp. 239–240.

[44] M. Karlsson, "Four-wave mixing in fibers with randomly varying zero-dispersion wavelength," *J. Opt. Soc. Amer. B*, vol. 15, no. 8, pp. 2269–2275, 1998.

[45] J. M. Chávez Boggio and H. L. Fragnito, "Simple four-wave-mixing-based method for measuring the ratio between the third- and fourth-order dispersion in optical fibers," *J. Opt. Soc. Amer. B*, vol. 24, no. 9, pp. 2046–2054, 2007.

[46] B. P.-P. Kuo, J. M. Fini, L. Grüner-Nielsen, and S. Radic, "Dispersion-stabilized highly-nonlinear fiber for wideband parametric mixer synthesis," *Opt. Exp.*, vol. 20, no. 17, pp. 18611–18619, 2012.

[47] B. P.-P. Kuo, M. Hirano, and S. Radic, "Continuous-wave, short-wavelength infrared mixer using dispersion-stabilized highly nonlinear fiber," *Opt. Exp.*, vol. 20, no. 16, pp. 18422–18431, 2012.

[48] B. P.-P. Kuo, N. Alic, P. F. Wysocki, and S. Radic, "Simultaneous wavelength-swept generation in nir and swir bands over combined 329-nm band using swept-pump fiber optical parametric oscillator," *J. Lightw. Technol.*, vol. 29, no. 4, pp. 410–416, Feb. 15, 2011.

[49] E. Myslivets and S. Radic, "Spatially-resolved characterization of dispersion flattened nonlinear fiber," *IEEE Photon. Technol. Lett.*, vol. 25, no. 5, pp. 434–437, Mar. 1, 2013.

[50] F. Gholami, E. Myslivets, S. Zlatanovic, N. Alic, and S. Radic, "Dispersion characterization of highly nonlinear fiber over a 700-nm band," *IEEE Photon. Technol. Lett.*, vol. 24, no. 12 pp. 1021–1023, Jun. 15, 2012.

[51] E. Myslivets, and S. Radic, "Advanced fiber optic parametric synthesis and characterization," in *Proc. Opt. Fiber Commun. Conf. Expo. Nat. Fiber Opt. Eng. Conf.*, Mar. 2011, pp. 1–3.

[52] E. Myslivets, C. Lundström, J. M. Aparicio, S. Moro, A. O. J. Wiberg, C.-S. Bres, N. Alic, P. A. Andrekson, and S. Radic, "Spatial equalization of zero-dispersion wavelength profiles in nonlinear fibers," *IEEE Photon. Technol. Lett.*, vol. 21, no. 24, pp. 1807–1809, Dec. 15, 2009.

Authors' biographies not available at the time of publication.